The Multi-INstrument Burst ARchive (MINBAR): data release 1

D. K. Galloway[1]
School of Physics & Astronomy, Monash University, Clayton VIC 3800, Australia

Jean in 't Zand
SRON Netherlands Institute for Space Research

Jérôme Chenevez
DTU Space, Lyngby, Denmark

Hauke Wörpel
Leibniz-Institut für Astrophysik, Potsdam

Laurens Keek
Department of Astronomy, University of Maryland, College Park, MD 20742, USA

Celia Sanchez-Fernandez and Erik Kuulkers
ESAC, Spain

Laura Ootes and Anna Watts
Anton Pannekoek Institute, University of Amsterdam
and

Luis Gisler
School of Physics & Astronomy, Monash University, Clayton VIC 3800, Australia

Abstract

We present the largest sample of type-I (thermonuclear) X-ray bursts ever assembled, encompassing 7057 bursts from 85 distinct sources. The sample has been compiled from observations with Xenon proportional counters on several long-duration satellites, including the *Rossi X-ray Timing Explorer*, *BeppoSAX*, and *INTEGRAL*. In addition to the burst sample, we include a companion sample with analysis results on every X-ray observation of burst sources by these instruments through 2012 May 3, totalling 117880 separate measurements. We also include analysis of the burst oscillations in the bursts observed with *RXTE*. We present a description of the sample, some basic analysis and ideas for further studies.

Subject headings: to be set

8. Observation catalog

The observation table contains information about public *RXTE*, *BeppoSAX* and *INTEGRAL* observations of the burst sources described in §2, based on the selection criteria defined in §3.1.1, §3.2.1 and §3.3.1. In addition to the criteria for the individual instruments, we filtered our analysis results to list only observations in which at least one source was detected (based on the average count rate) at 3σ significance, or higher.

The selection criteria for each instrument were adopted to achieve a sample that was largely (but not strictly) complete. For *RXTE* and *BeppoSAX*, completeness is in principle achievable, because the available public data extends through the end of each mission. For *INTEGRAL*, the observations are extracted from public data through revolution 1166 (MJD 56050).

We estimated the exposure for each observation based on the "good-time" intervals adopting standard screening criteria **JZ: please confirm for SAX and JEM-X? – dkg**

For *RXTE*, we analysed observations where one or more burst source was within the field of view, totalling 46.08 Ms (17900 observations). After the selection for the observations where a source was detected at the 3σ level or higher, we retained observations totalling 42.71 Ms.

We analysed a total of 14545 *BeppoSAX*/WFC observations, totalling 224.1 Ms. **JZ: comment here on what we do with sources that were detected as having bursts, after the end of mission – dkg**. The total exposure including significantly-detected sources is 133.6 Ms.

For *INTEGRAL*, we selected every public observation of burst sources through revolution 1166 (MJD 56050), totalling 605.7 Ms (245328 observations). Because we only searched for bursts through revolution 1166, we exclude from the observation table those sources with bursts first detected after this date. The accumulated exposure for observations with JEM-X with detections at 3σ significance is 268.7 Ms.

During the first two years following the launch of *INTEGRAL*, the JEM-X instruments could adopt an alternative "restricted imaging" mode, which was automatically activated to reduce the telemetry in case of increased count rates. This restricted mode, with only eight **jc: energy?** channels, was abandoned in 2004 and has not been supported by the OSA software since 2006. Therefore, any observations or bursts that occurred in this restricted mode could not be analysed for MINBAR.

We identified 114 science windows (through revolution 163) that were taken in "restricted imaging" mode, of which 99 included at least one burster. **remark: include a table listing the science windows and start, end times? – dkg** Including all the burst sources within 5° of the aimpoint of each affected science window, and based on the median length of science windows in the MINBAR observation catalog of 2 ks, the total exposure was 4.4 Ms (about 0.7% of the total 605.7 Ms of JEM-X observations that were analysed). For individual sources, the fraction of observations in this mode may have been as high as a few percent, but does not factor in the transient source activity, so may not have meant any significant loss of bursts. We further explore the effect of this data taking mode on the burst sample in §9.

The observations table includes a combined total of 117880 *RXTE*, *BeppoSAX* and *INTEGRAL* observations.

8.1. Table format

The observation table columns are listed in Table 5. Below we describe in more detail how the column entries relate to the analysis in §4.

1. Burster name (`name` in the web table) The target for the observation. For the imaging instruments, we present analysis results for lightcurves and spectra extracted for each source within the FOV. For *RXTE*, we list the source closest to the aimpoint in the case of multiple sources within the FOV, and/or the only active source within the FOV **dg: need to clarify how this was done, and/or refer back to the relevant section in the /xte analysis**.

2. Instrument label (`instr`) The instrument label is encoded as a three-character string. The first two characters correspond to the satellite and instrument, i.e.

- `XP`: *RXTE*/PCA

- `IJ`: *INTEGRAL*/JEM-X
- `SW`: *BeppoSAX*/WFC

The third character corresponds to the camera number (for the WFC and JEM-X; see §3.2 and §3.3, respectively). For JEM-X observations later in the mission, both instruments were active; these are indicated by instrument code `IJX`, and the provided attributes are an average over the results for the two cameras individually (see §4.1). For the PCA, the third character encodes the number of PCUs active, with the possible values listed in Table 6. To summarise briefly, the number of PCUs on can be inferred from

1. a digit 0–4 corresponds to only that PCU operating
2. two-PCU observations are labeled b, c, d, f, g, i, m, n, p and t
3. three-PCU observations e, h, j, k, o, q, r, u, v, x
4. four-PCU observations, l, s, w, y and z
5. letter "a" corresponds to all five PCUs functional

3. Observation ID (`obsid`) The identifier for each observation is allocated by the science team. For *BeppoSAX*, this attribute corresponds to the observation period ('OP') which identifies a contiguous observation with a constant pointing.

For *INTEGRAL*, each observation corresponds to a science window each with a unique observation ID. This attribute is a 12-digit number of the form `RRRRPPPPSSSF`, where `RRRR` is the revolution number of the S/C as defined from perigee passage; `PPPP` is the pointing number within the revolution (reset to `0000` when the revolution number increments; `SSS` is the subdivision number, beginning at `001` and resetting on each new pointing; and `F` is the type identifier of the science window, with allowed values of 0 ("pointing"), 1 ("Slew"), and 2 ("Engineering"). For the observations included in the sample here, we selected only the "Pointing" type (`F=0`).

For *RXTE*, the observation ID is of the form `NNNNN-TT-VV-SS[X]` where: `NNNNN` is the five-digit proposal number assigned by the guest observer facility (GOF); `TT` is a two-digit target number, which may be zero if there was only one target for the proposal; `VV` is the two-digit viewing number, assigned by GOF, which tracks the number of scheduled visits (epochs) for each target; `SS` is the two-digit sequence number used for identifying different pointings that make up the same viewing (if the viewing was further split into more than one interval); and `X` the optional 15th character, which when present, indicates: `S` "raster" scan observation or `R` "raster" grid observation.

4. MINBAR observation ID (`entry`) The unique numeric identifier for each observation in the MINBAR sample.

5. Analysis flags (`flag`) Indicates a number of sub-optimal situations for the data analysis, as described in Table 4. **dg: note alternate format in web table**

6 & 7. Observation start and end times (`tstart, tstop`) The nominal extent of each observation, in MJD. Data may not be continuous throughout the interval, due to occultations, passages through regions of high particle flux, or other instrumental factors.

8. Total exposure (`exp`) The total on-time for the observation, taking into account the data gaps.

9. Off-axis angle (`angle`) The angle (in arcmin) between the instrument aimpoint and the source position.

10. Vignetting correction factor (`vigcorr`) The factor describing what fraction of the detector can 'see' the source within the confines of the entrance window.

For *RXTE*, we generated a separate response matrix for each observation factoring the position of the source within the FOV, so this input implicitly takes into account the (approximately linear) decrease in instrumental sensitivity moving away from the aimpoint.

11. Number of (type-I) bursts detected in the observation (`nburst`) This is the total

TABLE 4
ANALYSIS FLAGS RELEVANT TO MINBAR OBSERVATIONS

Label	Instrument	Description
-	all	No significant analysis issues
a	*RXTE*	Multiple sources active in the field, but sources other than the named source contribute negligible flux
b	*RXTE*	Multiple sources active in the field and sources other than the named origin contribute non-negligible flux
c	*RXTE*	Multiple sources active in the field and no information is available about the relative intensities
d	*RXTE*	Standard filtering left no good times
e	*RXTE* & *INTEGRAL*	No Standard-2 mode data, or no spectrum available
f	*RXTE*	No FITS data available in archive

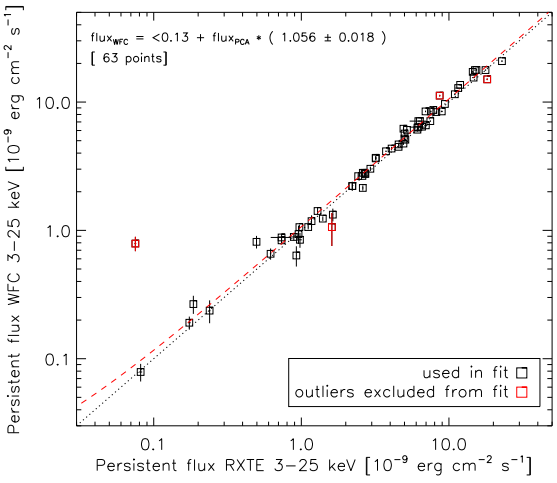

Fig. 4.— Cross-calibration for the 3–25 keV flux for overlapping observations with *BeppoSAX*/WFC and *RXTE*/PCA in the MINBAR observation table. The dotted line shows a 1:1 correspondence; other elements as for Fig. 3

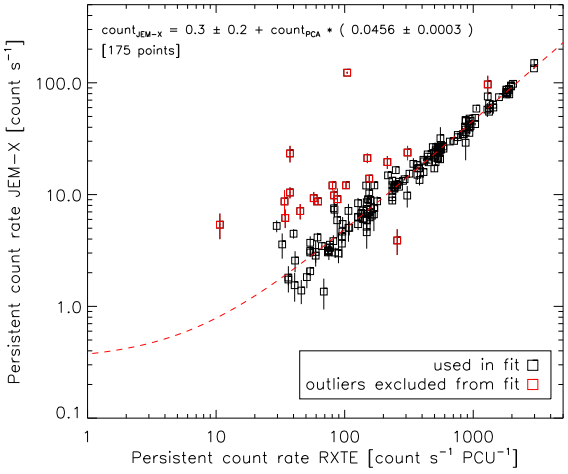

Fig. 5.— Cross-calibration for the mean count rate for overlapping observations with *INTEGRAL*/JEM-X and *RXTE*/PCA in the MINBAR observation table. The points which are excluded from the fit are marked (*red symbols*); the line of best-fit is overplotted (*dashed red line*).

number of bursts **dg: from this source?** detected in the observation. There may be additional weakly-significant candidates which could not be confirmed as bursts.

12 & 13. Count rate and error (`count`, `counte`) The background-subtracted count rate (and 1σ uncertainty) averaged over the entire ob-

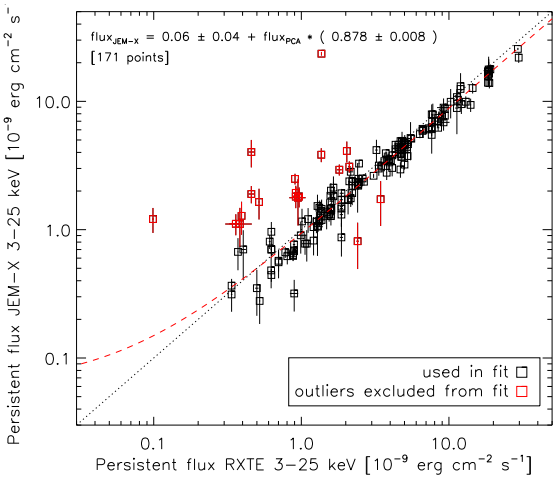

Fig. 6.— Cross-calibration for the 3–25 keV flux for overlapping observations with *INTEGRAL*/JEM-X and *RXTE*/PCA in the MINBAR observation table. The dotted line shows a 1:1 correspondence; other elements as for Fig. 3.

servation. For JEM-X observations where both cameras are operational, we average over JEM-X 1 and 2. For the PCA, we give the count rate per active PCU.

14. Detection significance (`sig`) The estimated detection significance for this source in the observation. This is calculated as **dg: check** the background rate divided by the uncertainty. We only include observations in the table where the detection is at least at the (estimated) 3σ level, although this quantity is not always available for instrumental reasons. We also include any observations in which a burst has been detected **dg: may need to double check these**.

15 & 16. Mean persistent flux for the observation (`flux, fluxe`) This attribute is the integrated flux F_p and uncertainty in units of 10^{-9} erg cm^{-2} s^{-1}, based on the spectral model given in column 23, and the best-fit spectral parameters in columns 24–45.

17 & 18. Energy range for flux measurements (`emin, emax`) The integration limits for the flux measurement given in columns 15 & 16.

19. The γ-value (`gamma`) This attribute is the persistent flux F_p (column 15) divided by the inferred Eddington flux for the source, i.e. column 3 of Table 2; after van Paradijs et al. (1988)

20 & 21. The soft & hard spectral colours (`sc, hc`) These attributes parametrise the shape of the persistent spectrum, and are derived from the best-fit spectral model, as described in §4.3.

22. The S_Z parameter (`s_z`) This attribute quantifies the position on the colour-colour diagram, for those sources with observations spanning sufficient range of spectral shapes to describe it (see §4.3).

23. The spectral model (`model`) This column specifies the spectral model adopted for the persistent spectrum, in XSPEC format (Dorman & Arnaud 2001). See §4.1 for a description of how the spectral models were chosen. Columns 24–45 list the spectral parameters corresponding to the adopted model, with columns 24–27 describing the power-law component, where present; 28–31 the blackbody component; 32–39 the Comptonisation component; and 40–45 the Gaussian component. **dg: note alternate arrangement in the online table** Where no spectral information was available, or no good fit could be obtained **dg: any examples of this?** this attribute is blank.

24 & 25. Power law spectral index and uncertainty For those observations with a power-law component, we list here the best-fit spectral index and uncertainty.

26 & 27. Power law normalisation The best-fit normalisation and uncertainty of the power-law component, where present.

28 & 29. The blackbody temperature For those observations with a blackbody component, we list in these columns the best fit temperature kT and uncertainty in keV.

30 & 31. The blackbody normalisation The best fit normalisation and uncertainty for the blackbody, where present.

32 & 33. The Comptonisation component seed photon temperature For those observations with a Comptonisation continuum component, we list in these columns the best-fit seed photon (Wien) temperature, T_0 and uncertainty, in keV.

34 & 35. The Comptonisation plasma temperature The best-fit plasma temperature kT and uncertainty. This attribute (and the optical depth τ, below) are measured with a fixed "geometry" flag for the `compTT` component of 1.0, corresponding to the default "disk" geometry

36 & 37. The Comptonisation optical depth The best-fit optical depth τ for scattering for those observations including a Comptonisation component.

38 & 39. The Comptonisation component normalisation The best-fit normalisation and uncertainty of the `compTT` component, where present.

40 & 41. The energy of the Gaussian For those observations with a Gaussian component (simulating Fe Kα emission around 6.4–6.7 keV), we list here the best-fit line energy (and uncertainty). **dg: mention the limits? or refer to in the spectral fitting section**

42 & 43. The Gaussian width The best-fit width σ and uncertainty of the Gaussian component, where present.

44 & 45. The Gaussian normalisation The best-fit normalisation of the Gaussian component and estimated uncertainty, where present.

46 & 47. The fit statistic (`chisqr, chisqre`) The reduced χ^2_ν ($\equiv \chi^2/\nu$, where ν is the number of degrees of freedom in the fit). Where more than one spectrum were used for a simultaneous fit (e.g. for the case of the *RXTE*/PCA where multiple PCUs were operational) we list the mean χ^2_ν and the standard deviation.

8.2. Observation summary

Here we list some descriptive parameters for the observation table.

We show in Figure 7 the cumulative exposure over the history of each mission. The total exposure over all the sources was 133.6 Ms, 268.7 Ms, and 42.71 Ms for *BeppoSAX*/WFC, *INTEGRAL*/JEM-X and *RXTE*/PCA, respectively. The 6-monthly "steps" visible in the curves for *BeppoSAX* and *INTEGRAL* are related to the annual periods of visibility of the Galactic centre. The exposure for *RXTE* increases at a lower, although more steady rate over the mission lifetime.

The concentration of sources around the Galactic centre, and the corresponding observational focus on that area, results in a strong dependence of total exposure on angular distance from the centre. Most sources within 5° of the Galactic centre have accumulated 15 Ms of total exposure. For sources more than 5° away, 1–10 Ms is more typical.

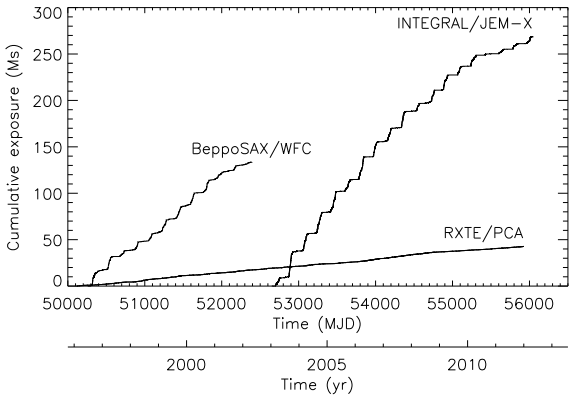

Fig. 7.— Cumulative exposure for each of the three missions comprising the MINBAR observation sample.

We show the exposure as a function of γ-value in Figure 8. This quantity is the ratio of the persistent flux F_p to the average peak flux of radius-expansion bursts (for those sources where they are observed; see §4.6). It is understood to be proportional to the accretion rate, up to a factor of approximately $c_{\rm bol}\xi_p/\xi_b$, where $c_{\rm bol}$ is the required bolometric correction to the band-limited persistent flux, and $\xi_{p,b}$ are the anisotropy factors for the persistent and burst emission, respectively (follow-

TABLE 5

OBSERVATION TABLE COLUMNS, FORMATS **dg: may not all be correct – check!** AND DESCRIPTION

Column	Web table attribute	ASCII table Format	Units	Description
1	`name`	A23		Burster name
2	`instr`	A6		Instrument label
3	`obsid`	A20		Observation ID
4	`entry`	I6		MINBAR observation ID
5	`flag`	A3		Analysis flags
6	`tstart`	F11.5	MJD	Observation start time
7	`tstop`	F11.5	MJD	Observation stop time
8	`exp`	I6	s	Total exposure
9	`angle`	F7.2	arcmin	Off-axis angle
10	`vigcorr`	F5.3		Vignetting correction factor
11	`nburst`	I3		Number of (type-I) bursts in the observation
12	`count`	F6.3	count s^{-1}	Background-subtracted mean rate for target source
13	`counte`	F6.3	count s^{-1}	Uncertainty[a] on mean rate
14	`sig`	F6.1		Detection significance for this observation
15	`flux`	F6.3	10^{-9} erg cm^{-2} s^{-1}	Mean flux over the observation
16	`fluxe`	F6.3	10^{-9} erg cm^{-2} s^{-1}	Estimated uncertainty[a] on mean flux
17	`emin`	F5.1	keV	Minimum of energy band for observation-averaged flux (and spectral fit)
18	`emax`	F5.1	keV	Maximum of energy band for observation-averaged flux (and spectral fit)
19	`gamma`	F6.4		γ ratio of persistent flux to mean peak flux of radius-expansion bursts
20	`sc`	F6.3		Soft colour
21	`hc`	F6.3		Hard colour
22	`s_z`	F6.3		S_Z value, giving position in the colour-colour diagram
23	`model`	A30		Spectral model (XSPEC syntax)
24		F5.3		Spectral index of power law (where present)
25		F5.3		Uncertainty[a] on spectral index
26		F5.3	photons keV^{-1} cm^{-2} s^{-1} at 1 keV	Normalisation of power law (where present)
27		F5.3	photons keV^{-1} cm^{-2} s^{-1} at 1 keV	Uncertainty[a] on power-law normalisation
28		F5.3	keV	Temperature kT of blackbody component (where present)
29		F5.3	keV	Uncertainty[a] on blackbody temperature
30		F5.3	$(R_{\rm km}/d_{10\ \rm kpc})^2$	Normalisation of blackbody component (where present)
31		F5.3	$(R_{\rm km}/d_{10\ \rm kpc})^2$	Uncertainty[a] on blackbody normalisation
32		F5.3	keV	Input soft photon (Wien) temperature T_0 of Comptonisation component (where present)
33		F5.3	keV	Uncertainty[a] on Comptonisation input temperature T_0
34		F5.3	keV	Plasma temperature kT of Comptonisation component (where present)
35		F5.3	keV	Uncertainty[a] on Comptonisation plasma temperature
36		F5.3		Plasma optical depth τ of Comptonisation component (where present)
37		F5.3		Uncertainty[a] on Comptonisation optical depth
38		F5.3		Normalisation of Comptonisation component (where present)
39		F5.3		Uncertainty[a] on Comptonisation normalisation
40		F5.3	keV	Line energy for Gaussian component (where present)
41		F5.3	keV	Uncertainty[a] on Gaussian line energy
42		F5.3	keV	Line width σ for Gaussian component (where present)
43		F5.3	keV	Uncertainty[a] on Gaussian line width
44		F5.3	photons cm^{-2} s^{-1}	Normalisation for Gaussian component (where present)
45		F5.3	photons cm^{-2} s^{-1}	Uncertainty[a] on Gaussian line normalisation
46	`chisqr`	F5.2		Mean reduced χ^2 of spectral fits
47	`chisqre`	F5.2		Standard deviation of reduced χ^2 from spectral fits, where more than one spectrum is fit

[a]Uncertainties are at the 1-σ (68%) confidence level

TABLE 6
RXTE/PCA INSTRUMENT CODES

Label	PCUs active
0	0
1	1
2	2
3	3
4	4
b	0, 1
c	0, 2
d	1, 2
f	0, 3
g	1, 3
i	2, 3
m	0, 4
n	1, 4
p	2, 4
t	3, 4
e	0, 1, 2
h	0, 1, 3
j	0, 2, 3
k	1, 2, 3
o	0, 1, 4
q	0, 2, 4
r	1, 2, 4
u	0, 3, 4
v	1, 3, 4
x	2, 3, 4
l	0, 1, 2, 3
s	0, 1, 2, 4
w	0, 1, 3, 4
y	0, 2, 3, 4
z	1, 2, 3, 4
a	0, 1, 2, 3, 4

ing Fujimoto 1988). $c_{\rm bol}$ is typically in the range 1.1–2, depending on the source spectral state. The inclination factor ξ_p/ξ_b varies between 0.6–1.8 for low-inclination (non-dipping) systems, or up to 2.3 for dipping systems ($i \approx 75°$; He & Keek 2016).

We find that the inferred accretion rate peaks at around $0.1\dot{m}_{\rm Edd}$, ranging over almost two orders of magnitude higher and lower. The lower range, 0.01–$0.1\dot{m}_{\rm Edd}$, is typically where the ultracompact sources fall, while the highest values, $\gamma > 1$, are dominated by the Z-sources.

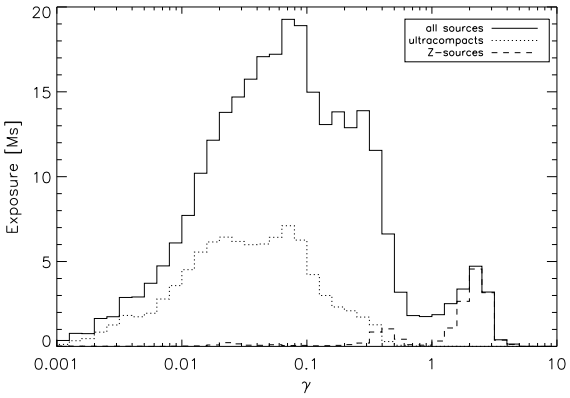

Fig. 8.— Exposure as a function of γ-value (proportional to the accretion rate in units of $\dot{m}_{\rm Edd}$), both for the entire MINBAR sample, and the subsamples comprised of the ultracompact sources (and candidates), and the Z-sources (see §2).

- show an exposure map?
- breakdown of spectral models, χ^2-values, and ranges of spectral parameters?

9. Burst catalog

The burst table contains analysis results for every *RXTE*, *BeppoSAX* and *INTEGRAL* burst from the sources described in §2, detected in the observations making up the observation table (§8).

The degree of completeness of our sample depends on both the selection of observations that comprise our search scope (see §8), but also the probability of unambiguously detecting each burst within each observation. There are a number of instances which might result in bursts occurring during the observation intervals of the three instruments, being overlooked by our search strategy. First, the burst may simply be too faint, or observed at too large an angle from the instrument aimpoint. In such cases it is challenging to confirm the presence of weak bursts, except where there is other corroborating evidence for the events. Such evidence may include the detection of the event by an instrument other than the three used for this sample, or a predicted event based on a series of events with a regular recurrence time.

Second, the good time intervals over which our lightcurves are extracted may not encompass the entire period in which a particular source is observed (and in which bursts may be detected). For *RXTE*, we select only those observations for which a burst source is within 0.°6 of the instrument aimpoint, as described in §8 **dg: needs to be revised – check!**. It is possible that observations of bursts sources further off-axis may yield additional events that are not part of the current sample. For the other instruments, it is possible that different choices for the criteria defining the good-time intervals, and/or longer-term variations in the data extraction algorithm arising from software version changes, may result in more conservative observation intervals.

Third, there were a number of instrumental issues that prevented some data being analysed for the MINBAR sample. **jc: please check and confirm details – dkg** For JEM-X, some of the early data from the mission was taken in a (now deprecated) "restricting imaging mode", for which the current version of the OSA software (10) cannot produce lightcurves (or spectra; see §8). Notable events that are affected by this issue include the long burst from SLX 1735−269 on MJD 52897.733 (see Molkov et al. 2005; in't Zand & Weinberg 2010). **dg: need a better estimate here of the number of bursts that might have been missed?**

We performed a number of tests to ensure the completeness of the data. First, we cross-matched the events seen in each instrument, with any overlapping observations by the other instrument... **dg: to fill in**

Second, we compared our detected sample with smaller sub-samples reported in the literature. For example, Falanga et al. (2006) analysed 36 bursts detected with *INTEGRAL*/JEM-X or ISGRI from 4U 1728−34. Upon cross-matching the burst times with those in MINBAR, we uncovered two

events (#7 and 12) which were not identified in the JEM-X lightcurve search. **cs: maybe explain why, were they too weak? maybe too short? - dg** Seven further events reported by those authors were not covered by lightcurves extracted for MINBAR **cs: are there any more light curves missing? this should be checked - jc**. We also note two events (#31 and 35) for which the lightcurves analysed for MINBAR do not show any evidence for a burst. **dg: other things to mention here: comparison with Tullio's sample; comparison with the Aranzana et al. (2016) sample; Chelovekov's samples; and keep in mind the issue with the missing SLX 1735-269 burst(s)**

Third, we analysed selected groups of bursts observed close together in time, to determine whether they were consistent with a regular recurrence time. **dg: to fill in**

jc: Add discussion here on effect of the off-axis angle on the flux measurements

9.1. Table format

The burst table columns are listed in Table 8. Below we describe in more detail how the column entries relate to the analysis in §4.

1–3 These attributes are identical to the corresponding columns in the observation table (see §8).

4. Burst start time (`time`) The burst start time, in MJD UT, as defined in §4.4.2.

5. MINBAR burst ID (`entry`) The unique identifier for each burst in the MINBAR sample.

6. MINBAR observation ID (`obsid`) The unique identifier of the observation in the observation table in which this burst was detected.

7. Order of the burst in this observation (`bnum`) The ranking in time order of this event in the entire observation. For *BeppoSAX*, the ranking includes each burster in the FOV; the ranking may be incidentally out of order.

8. Burst number in the G08 catalog This attribute is the corresponding entry value in the catalog of bursts detected with *RXTE* (G08).

9. Number of independent detections (`mult`) There is a small number of bursts detected simultaneously by more than one instrument. For these events, we set this attribute to 2. For other bursts, it is 1.

10. Off-axis angle (`angle`) The angle (in arcmin) between the instrument aimpoint and the source position, as for the observation table (see §8). This may be different from the value in the corresponding observation, for *RXTE* observations which include multiple sources in the FOV.

11. Vignetting correction factor (`vigcorr`) The factor assumed in the analysis procedure by which the count rate and other quantities are scaled to take into account the instrumental vignetting, as for the observation table (§8).

12. Data quality/analysis flag (`flag`) Indicates a number of sub-optimal situations for the data analysis, as described in Table 7. **dg: note alternate format in web table**

13. Photospheric radius-expansion (`rexp`) This attribute indicates the presence of photospheric radius expansion (PRE), as assessed from the time-resolved spectroscopy. The possible entries are Y/N, indicating confirmed presence/absence (respectively); M indicating marginal evidence; ? indicating insufficient data to assess **dg: and X indicating we haven't checked; need to fix these**.

14 & 15. Rise time & uncertainty (`rise`, `risee`) The burst rise time estimated from the lightcurve analysis, as described in §4.4.2.

16 & 17. Burst timescale τ (`tau`, `taue`) The ratio of the burst fluence to peak flux, $\tau = E_b/F_{\rm peak}$, and the estimated uncertainty.

Table 7
Analysis flags relevant to MINBAR bursts

Label		Description
-	all	No significant analysis issues
a	*RXTE*	The burst was observed during a slew, and thus offset from the source position.; fluxes and fluence have been scaled by $1/(1-\Delta\theta)$
b	*RXTE*	The observation was offset from the source position; flux and fluence have been adjusted via setting the source position for response matrix generation
c	*RXTE*	The origin of the burst is uncertain; the burst may have been from another source in the field of view. If the origin is not the centre of the FOV, the flux and fluence have been adjusted by calculating the response for the assumed source position
d	*RXTE*	Buffer overruns (or some other instrumental effect) caused gaps in the high time resolution data
e	*RXTE*	The burst was so faint that only the peak flux could be measured, and not the fluence or other parameters; or, alternatively, that the burst was cut off by the end of the observation, so that the fluence is an underestimate
f	*RXTE*	An extremely faint burst or possibly problems with the background subtraction, resulting in no time-resolved spectral fit results
g	all	The full burst profile was not observed, so that the event can be considered an unconfirmed burst candidate. Typically in these cases the initial burst rise is missed, so that the measured peak flux and fluence are lower limits only
h	*RXTE*	High-time resolution modes don't cover burst, preventing any time-resolved spectroscopic results

18 & 19. Burst duration (`dur, dure`) The approximate duration of the burst, and its uncertainty.

20 & 21. Exponential decay timescale (`edt, edte`) The decay timescale and uncertainty for an exponential fit to the intensity lightcurve.

22. Time since previous burst (`tdel`) The elapsed time since the previous burst from this source.

23. Inferred recurrence time (`trec`) The recurrence time inferred for the burst. This quantity may be different from the elapsed time since the previous bursts, in cases where we infer a steady recurrence time with undetected bursts falling in data gaps. **dg: should really also have an error**

24 & 25. Pre-burst persistent flux (`perflx, perflxe`) The estimated persistent flux and uncertainty immediately prior to the burst. This quantity may be identical to the value inferred for the entire observation, but in some cases we estimate fluxes from spectra extracted over shorter intervals.

26 & 27. Energy range for the persistent flux (`emin, emax`) The energy range over which the pre-burst persistent flux is integrated.

28 & 29. Burst α-value (`alpha, alphae`) This quantity is the ratio of integrated persistent flux (i.e. $\Delta t F_{\rm pers}$) to the burst fluence, E_b, and also incorporates the bolometric correction factor (column 30).

30 & 31. Bolometric correction factor (`bc, bce`) The estimated correction factor (and uncertainty) by which the persistent flux needs to be multiplied for the best estimate of the bolometric flux.

32. γ-value (`gamma`) The ratio of the persistent flux to the average Eddington flux from the source (from Table 2).

33 & 34. Soft & hard spectral colour (`sc, hc`) The soft and hard spectral colours calculated over the entire observation; these are duplicated from the observation table (§8).

35. Position on colour-colour diagram S_Z (`s_z`) This attribute is also calculated from the observation table, and is copied here.

36 & 37. Peak count rate (`pcount, pcounte`) The peak count rate and uncertainty for the event.

38 & 39. Peak intensity (`pflux, pfluxe`) The peak intensity and uncertainty, calculated from the count rate rescaled by the adopted instrumental effective area (see §4.4.2).

40 & 41. Integrated intensity (`fluen, fluene`) The integrated intensity over the burst duration. This quantity is expected to be approximately proportionally to the bolometric fluence.

42 & 43. Energy range for intensity (`emin, emax`) The energy range over which the intensities are measured.

44 & 45. Bolometric peak flux (`bpflux, bpfluxe`) The estimated peak bolometric flux of the burst, based on the parameters determined from time-resolved spectroscopy.

46 & 47. Blackbody temperature at burst peak (`kT, kTe`) The best-fit value of the blackbody temperature kT and its uncertainty, for the spectrum with maximum bolometric flux.

48 & 49. Blackbody normalisation at burst peak (`rad, rade`) The best-fit value of the blackbody normalisation and its uncertainty, for the spectrum with maximum bolometric flux. **dg: check units here**

50 & 51. Bolometric fluence (`bfluen, bfluene`) The integrated bolometric flux over the entire burst duration.

52. References for the burst Here we indicate prior analyses in the literature which included or focussed on this event. References are numbered, and may be matched with the list below:

1. Kuulkers et al. (2003); 2. Kuulkers et al. (2010); 3. in't Zand & Weinberg (2010); 4. in't Zand et al. (2014b); 5. Chelovekov et al. (2005); 6. Aranzana et al. (2016); 7. in 't Zand et al. (2005b); 8. Cornelisse et al. (2002b); 9. Jonker et al. (2001); 10. in 't Zand et al. (2008); 11. Bhattacharyya (2007); 12. in't Zand et al. (2003); 13. Barnard et al. (2001); 14. Linares et al. (2010); 15. Cornelisse et al. (2003); 16. Strohmayer et al. (1998b); 17. Miller (1999); 18. Miller (2000); 19. Giles et al. (2002); 20. Muno et al. (2002); 21. Galloway et al. (2006); 22. Bhattacharyya & Strohmayer (2006a); 23. Jonker et al. (2004a); 24. Wijnands et al. (2001); 25. Wijnands et al. (2002b); 26. Markwardt et al. (1999); 27. in 't Zand et al. (2005a); 28. Ford et al. (1998); 29. Agrawal et al. (2001); 30. Kuulkers et al. (2009); 31. Kaptein et al. (2000); 32. Molkov et al. (2000); 33. Suleimanov et al. (2011); 34. Franco (2001); 35. van Straaten et al. (2001); 36. Galloway et al. (2003); 37. Strohmayer et al. (1997b); 38. Strohmayer et al. (1998a); 39. Strohmayer et al. (1996); 40. Falanga et al. (2006); 41. Fox et al. (2001); 42. Guerriero et al. (1999); 43. Muno et al. (2000); 44. in 't Zand et al. (2002); 45. Strohmayer et al. (1997a); 46. Werner et al. (2004); 47. den Hartog et al. (2003); 48. Kuulkers & van der Klis (2000); 49. in 't Zand et al. (1999b); 50. Jonker et al. (2000); 51. Galloway et al. (2004a); 52. Kaaret et al. (2002); 53. in 't Zand et al. (2003b); 54. in 't Zand et al. (2003a); 55. In't Zand et al. (1999); 56. Chelovekov & Grebenev (2007); 57. Cornelisse et al. (2007); 58. in 't Zand et al. (1998b); 59. in 't Zand et al. (2001); 60. Galloway & Cumming (2006); 61. Chakrabarty et al. (2003); 62. Bhattacharyya & Strohmayer (2006b); 63. Bhattacharyya & Strohmayer (2007); 64. Fiocchi et al. (2009); 65. Strohmayer et al. (2003); 66. Watts et al. (2005); 67. Kuulkers et al. (2002); 68. in 't Zand et al. (2004a); 69. Cocchi et al. (2001b); 70. Ubertini et al. (1999); 71. Galloway et al. (2004b); 72. Kong et al. (2000); 73. in 't Zand et al. (1998c); 74. Kajava et al. (2017a); 75. Zhang et al. (1998); 76. Galloway et al. (2001); 77. Tomsick et al. (1999); 78. Smale (2001); 79. Smale (1998); 80. Titarchuk & Shaposhnikov (2002).

9.2. Burst summary

10. Burst oscillations

Here we describe how the burst oscillation analysis described in §4.7 is presented in the MINBAR sample.

10.1. Table format

Below we list the table columns, units, and the format in the ASCII file. Column 9 is copied from the burst table (testing the row number cross-references here)

1–6 These attributes are identical to the corresponding columns in the burst table (see §9).

7. Number of bins $N_{\rm t}$

8. Estimated background rate $C_{\rm B}$ per PCU in the time range 20–5 seconds prior to the burst

9. Detection flag = 1 for a detection, or = 0 for no detection (in which case the following columns are limits)

10–12. Amplitude of signal and uncertainty given as %rms, with the 1σ lower and upper limit, respectively

13. Frequency of the signal to within a Hz.

14. Signal power of the detected oscillation Z^2_m

15. Power of the most-significant signal Z^2_s

16. Burst phase for detection (r)ise, (p)eak, (t)ail or (n)one

17. Detection criterion by which the time bin identified as having the most significant signal was selected; 1: single bin, not in the first second; 2: single bin, signal in the first second; 3–5: double time-frequency bin;

Table 8

Burst table columns, formats and description

Column	Web table attribute	ASCII table Format	Units	Description
1	name	A23		Likely source origin
2	instr	A3		Instrument label
3	obsid	A20		Observation ID
4	time	F11.5	MJD	Burst start time [UT]
5	entry	I4		MINBAR burst ID
6		I6		MINBAR observation ID in which this burst falls
7	bnum	I3		Order of the event in the observation
8		I3		Burst number in the G08 catalog
9	mult	I1		Number of independent detections
10	angle	F6.2	arcmin	Off-axis angle
11	vigcorr	F5.3		Vignetting correction factor
12	flag	I4		Data quality/analysis flag
13	rexp	A1		Photospheric radius expansion
14	rise	F5.2	s	Rise time
15	risee	F5.2	s	Uncertainty on rise time
16	tau	F5.1	s	Ratio of fluence to peak flux, $\tau = E_b/F_{\rm peak}$
17	taue	F5.1	s	Uncertainty on τ
18	dur	F6.1	s	Burst duration
19	dure	F6.1	s	Uncertainty on burst duration
20	edt	F5.1	s	Exponential decay timescale
21	edte	F5.1	s	Uncertainty on exponential decay timescale
22	tdel	F7.1	hr	Time since previous burst from this source
23	trec	F7.1	hr	Inferred recurrence time $T_{\rm rec}$
24	perflx	F6.3	10^{-9} erg cm^{-2} s^{-1}	Persistent flux prior to burst $F_{\rm per}$
25	perflxe	F5.3	10^{-9} erg cm^{-2} s^{-1}	Uncertainty on persistent flux
26	emin	F5.1	keV	Minimum of energy band for persistent flux
27	emax	F5.1	keV	Maximum of energy band for persistent flux
28	alpha	F6.1		Burst α-value
29	alphae	F6.1		Uncertainty on α
30	bc	F5.3		Bolometric correction adopted for persistent flux
31	bce	F5.3		Uncertainty on bolometric correction
32	gamma	F6.4		Ratio of persistent flux to peak PRE burst flux, γ
33	sc	F6.3		Soft colour
34	hc	F6.3		Hard colour
35	s_z	F6.3		Position on colour-colour diagram, S_Z
36	pcount	F6.1	count s^{-1}	Peak count rate
37	pcounte	F5.1	count s^{-1}	Error on peak rate
38	pflux	F6.2	count s^{-1} cm^{-2}	Peak intensity
39	pfluxe	F5.2	count s^{-1} cm^{-2}	Error on peak intensity
40	fluen	F6.4	count cm^{-2}	Integrated intensity
41	fluene	F6.4	count cm^{-2}	Error on integrated intensity
42	emin	F5.1	keV	Minimum of energy band for intensity
43	emax	F5.1	keV	Maximum of energy band for intensity
44	bpflux	F6.2	10^{-9} erg cm^{-2} s^{-1}	Estimated bolometric peak flux $F_{\rm peak}$
45	bpfluxe	F5.2	10^{-9} erg cm^{-2} s^{-1}	Uncertainty on bolometric peak flux
46	kT	F4.2	keV	Blackbody temperature kT at burst peak
47	kTe	F4.2	keV	Uncertainty on kT at burst peak
48	rad	F6.1	km/10 kpc	Blackbody normalisation at burst peak
49	rade	F5.1	km/10 kpc	Uncertainty on blackbody normalisation at burs peak
50	bfluen	F6.4	10^{-6} erg cm^{-2}	Estimated bolometric fluence E_b
51	bfluene	F6.4	10^{-6} erg cm^{-2}	Uncertainty on bolometric fluence
52		A10		References for the burst

18. First bin flag = 1 if the signal was found in the first time bin following the start

19 & 20. Time range for bin in seconds relative to the burst start time

10.2. Burst oscillation summary

Here we briefly describe the properties of the burst oscillation sample

lo: Do you want to add a brief summary here? – dkg

11. Discussion

11.1. Statistical properties

Discuss distribition of duration and classes of bursts.

Discuss recurrence time.

Discuss constraints on population of bursters in the galaxy, possible scaling to other galaxies.

Role of observation catalog (not previously provided, e.g. for Galloway et al. 2008); long-term behaviour, timescale and patterns for variation in spectral shapes etc.

11.2. Previously published results

In the following items, we summarize results that were obtained during the construction of MINBAR and were published previously. **remark: in random order, probably needs to be changed - jz**

11.2.1. Peculiar short recurrence times

Typical recurrence times between X-ray bursts are a few hours, which is consistent with theoretical ignition model predictions. However, much shorter recurrence times of order a few minutes have been measured in individual data runs, see for instance Boirin et al. (2007), which appeared inconsistent with theory. Keek et al. (2010) carried out a systematic analysis of all recurrence times for the 3387 bursts from PCA and WFC data that made up MINBAR at the time. 136 bursts have recurrence times of less than 1 hr, that come in multiples of up to four events, from 15 sources. Such short recurrence times are not present in data from the ultra-compact binaries. This suggests that hydrogen-burning processes play a crucial role in creating short recurrence times. As far as the neutron star spin frequency is known, these sources all spin fast at over 500 Hz. Rotationally induced mixing may explain burst recurrence times of the order of 10 minutes. Short recurrence time bursts generally occur at all mass accretion rates where normal bursts are observed, but for individual sources the short recurrence times may be restricted to a smaller interval of accretion rate. The fraction of such bursts is roughly 30%. The shortest known recurrence time is 3.8 minutes. **remark: This text has been adapted from the abstract of Keek et al. 2010 - jz** Recent numerical simulations explain this phenomenon as due to reignition of left-over hydrogen mixed into the ashes layer (**?**).

11.2.2. Burst evolution with transient m-dot evolution

dg: Analysis of burst behaviour during transient outbursts, specifically the hard-to soft transition, including IGR J17473−2721 (Chenevez et al. 2011) and GS 1826−24 (Chenevez et al. 2016) and perhaps also 4U 1728−34 (Kajava et al. 2017b). Also recent previous Science paper and Cavecchi 2017 paper.

One of the best-studied transient source in the MINBAR data sample is the so-called "textbook" burster, GS 1826-24. Indeed, this source was known as one of only two X-ray bursters to consequently agree with the expected steady-state behaviour for mixed H/He thermonuclear burning. Also known as the "Clocked Burster", GS 1826-24 has shown a regular burst recurrence time inversely proportional with the source accretion rate while in a persistent hard state until June 2014. At that time, the source switched into a softer state during which its burst behaviour changed from regular H-rich burning bursts to irregular, short helium bursts. One PRE burst was observed for the first time from this source by NuSTAR during this first soft episode, making it possible to derive a distance about 5.7 kpc (Chenevez et al. 2016, and references therein). Since then, GS 1826-24 has almost permanently remained in the soft state. All bursts included in the present MINBAR data release were observed by the WFC, JEM-X, and mainly the PCA, while the source was in the hard state (e.g. Galloway et al. 2004b).

TABLE 9

BURST OSCILLATION TABLE COLUMNS, FORMATS AND DESCRIPTION

Column	Format	Units	Description
1	A23		Burster name
2	A3		Instrument label
3	A20		Observation ID
4	F11.5	MJD	Burst start time [UT]
5	I5		MINBAR burst ID
6	I6		MINBAR observation ID
7	I2		Number of time bins exceeding the count threshold into which the burst was divided
8	F7.1	counts s^{-1} PCU^{-1}	Background rate estimated from the pre-burst emission
9	A1		Detection flag on burst oscillation; 1 for detection, 0 otherwise
10	F5.2	% rms	Amplitude of detected burst oscillation (or limit for non-detection)
11	F5.2	% rms	Lower error on amplitude
12	F5.2	% rms	Upper error on amplitude
13	I3	Hz	Frequency of the selected signal
14	F5.1		Signal power of the detected burst oscillation
15	F5.1		Measured power of the most-significant detected signal
16	A1		Phase during which oscillation was detected (peak phase=90% maximum); n = none, r = rise, p = peak, t = tail
17	I1		Detection criterion by which the highest-power signal was selected
18	I1		flag for signal found in the first bin after the burst start time?
19	F6.2	s	start time of the selected bin (relative to the burst start)
20	F6.2	s	time span of the selected bin

Chenevez et al. (2011) describe the bursting behaviour of the transient source IGR J17473-2721 during a six-month long outburst in 2008, which seemed to be triggered by the occurrence of a burst. The whole outburst was well covered by several instruments from start to end, making it possible to observe a wide range of accretion luminosities between 1% and 20% of Eddington. A total of 58 bursts were observed throughout the outburst, among which, one occurred simultaneously in both JEM-X and PCA. Two particularly interesting results can be stressed: 1) the burst activity dropped when the accretion rate reached 15% of Eddington, short before the peak of the outburst that was simultaneous with a sudden spectral change from hard to soft states. The burst activity resumed after one month, when the accretion rate returned below 5% of Eddington, thus demonstrating a hysteresis of burst rate vs. accretion rate. We note that similar burst intermissions have been registered from other bursting transients. One interpretation is the stabilization of the thermonuclear burning at high temperatures due to the heating of the neutron star crust by accretion, and the subsequent thermal relaxation of the crust delaying the resumption of unstable burning after the accretion rate reached back the level at which the burning stabilized. 2) The burst behaviour during the outburst exhibited seven phases across all burst regimes for H/He burning of Fujimoto et al. (1981), alternating between H-rich and pure helium burnings at hard and soft states, respectively, but at accretion rates 10 times higher than expected.

Bursts from the transient IGR J17254-3257 have been observed occurring at slightly different accretion rates but with very different durations. Chenevez et al. (2007) compare two bursts seen by JEM-X while the source was at a low accretion rate. The first burst observed from this source was short, at an accretion rate ¡0.5% of Eddington, thus consistent with helium burning triggered by hydrogen instability (Fujimoto et al. 1981; case 3). The other burst was observed with a duration of 15 minutes, typical of the cooling of a thick fuel layer, here interpreted as helium produced by hydrogen burning at low accretion rate (Peng et al. 2007). However, IGR J17254-3257 is an ultracompact X-ray binary candidate (in 't Zand et al. 2005) from which only H-poor accretion is expected. In such case, a more likely interpretation of the long burst would be the burning of a thick layer of pure helium slowly accreted from the degenerate companion onto the NS surface (e.g., Cumming et al. 2006).

jc: Should this be moved to the next sub-